Non-destructive phase contrast hard X-ray imaging to reveal the three-dimensional microstructure of soft and hard tissues

Anna Khimchenko[a], Georg Schulz[a], Hans Deyhle[a], Simone E. Hieber[a], Samiul Hasan[b], Christos Bikis[a], Joachim Schulz[b], Loïc Costeur[c], Bert Müller[a*]

[a]University of Basel, Biomaterials Science Center, Department of Biomedical Engineering, Gewerbestrasse 14, 4123 Allschwil, Switzerland;
[b]Microworks GmbH, Hermann-von-Helmholtz-Platz 1, 76344 Eggenstein-Leopoldshafen, Germany;
[c]Naturhistorisches Museum Basel, Augustinergasse 2, 4051 Basel, Switzerland

ABSTRACT

X-ray imaging in the absorption contrast mode is an established method of visualising calcified tissues such as bone and teeth. Physically soft tissues such as brain or muscle are often imaged using magnetic resonance imaging (MRI). However, the spatial resolution of MRI is insufficient for identifying individual biological cells within three-dimensional tissue. X-ray grating interferometry (XGI) has advantages for the investigation of soft tissues or the simultaneous three-dimensional visualisation of soft and hard tissues. Since laboratory microtomography (µCT) systems have better accessibility than tomography set-ups at synchrotron radiation facilities, a great deal of effort has been invested in optimising XGI set-ups for conventional µCT systems. In this conference proceeding, we present how a two-grating interferometer is incorporated into a commercially available nanotom® m (GE Sensing & Inspection Technologies GmbH) µCT system to extend its capabilities toward phase contrast. We intend to demonstrate superior contrast in spiders (*Hogna radiata* (*Fam. Lycosidae*) and *Xysticus erraticus* (*Fam. Thomisidae*)), as well as the simultaneous visualisation of hard and soft tissues. XGI is an imaging modality that provides quantitative data, and visualisation is an important part of biomimetics; consequently, hard X-ray imaging provides a sound basis for bioinspiration, bioreplication and biomimetics and allows for the quantitative comparison of biofabricated products with their natural counterparts.

Keywords: X-ray microtomography, phase contrast, grating interferometer set-up, laboratory-based microtomography systems.

1. INTRODUCTION

Biomimetics is a broad interdisciplinary field characterised by information transfer from nature to technical applications[1] and whose principle goal is to provide a deep understanding of strategies that evolve in nature. As processes and structures in nature are broad in length,[2] very often one has to work on the (sub-)microscopic level.[1] Nature has a complex three-dimensional (3D) hierarchical spatial form of organisation, and so 3D non-destructive quantitative visualisation with micrometer resolution is attractive for extracting structural and functional information.

Advantages in micro-computed tomography (µCT) have made it a highly effective technique for studying higher-density materials[3] down to the sub-micrometer level. The high-resolution visualisation of physically hard materials is successfully performed in the absorption contrast mode.[4,5] The challenge faced in visualising soft materials is low attenuation differences,[6] and so investigation of soft materials is based preferentially on staining and sectioning, or it is performed in the phase contrast mode. Phase contrast imaging is often successfully performed via synchrotron radiation-based micro-computed tomography (SRµCT); however, experiments at synchrotron facilities are sophisticated and impose severe time restrictions on the user.[7]

Nowadays, X-ray laboratory-based µCT systems are used widely in scientific research. However, the potential and flexibility of these systems are underestimated.[8] A great deal of effort has been invested in optimising grating

* bert.mueller@unibas.ch; phone: +41 61 207 54 30; fax: +41 61 207 54 99; bmc.unibas.ch

Bioinspiration, Biomimetics, and Bioreplication 2016, edited by Raúl J. Martín-Palma, Proc. of SPIE Vol. 9797, 97970B · © 2016 SPIE · CCC code: 0277-786X/16/$18 · doi: 10.1117/12.2222038

interferometry set-ups for laboratory-based X-ray tubes.[9,10] The present paper shows how a two-grating interferometer can be incorporated into a commercially available nanotom® m (GE Sensing & Inspection Technologies GmbH) µCT system, in order to extend its capabilities toward phase contrast. We intend to demonstrate superior contrast for lower-density materials, such as selected spiders, in the phase contrast mode, the possibility of simultaneously visualising soft and hard tissues using X-ray grating interferometry (XGI) and information gain from dark-field imaging on the example of mandible block. The spiders, namely (*Hogna radiata* (*Fam. Lycosidae*) and *Xysticus erraticus* (*Fam. Thomisidae*)), were selected as samples in this instance due to their relevance to biomimetics, for example, spider-inspired design can be found in robotics.[11,12] Grating-based phase contrast scans make it possible to reconstruct simultaneously the three-dimensional distribution of absorption (quantitative transmission), phase (quantitative refraction) and scattering (dark-field).[3] Thus, XGI can be understood as a 3D quantitative multi-modal methodology.

2. MATERIALS AND METHODS

2.1 Specimen preparation

Alcohol-fixed spiders were kindly provided from Natural History Museum Basel (NMB) collections, namely *Hogna radiata* (*Fam. Lycosidae*) and *Xysticus erraticus* (*Fam. Thomisidae*).

As a hard tissue specimen, a cylindrical mandible block from a five-month-old pig with two Ti implants (SLA surface, Straumann AG, Villeret, Switzerland), each 4.1 mm in diameter and 10 mm long, was used. Additional specimen information is described by M. Luckow et al.[13]

In order to evaluate the principle behind simultaneously visualising soft and hard tissues, a chicken wing was used. The wing was 5 cm long, consisting of a bony part with an approximate diameter of 1 cm and a soft tissue part with a maximal diameter of 4 cm.

2.2 Image formation: absorption versus phase contrast

Figure 1 shows a schematic set-ups used for absorption contrast (A) and grating-based phase contrast (B) imaging. Conventionally µCT measurements are performed in the absorption contrast mode. In this case, the signal in the reconstructed slices is related to linear attenuation within the sample[14] (see Holme et al. Box 1).

Using hard X-rays, attenuation variations in soft tissue samples are hardly visible, which in turn leads to poor image contrast. To overcome this problem, measurements can be performed in the phase contrast mode, in which an image signal is generated from distortions in the wavefront phase caused by the specimen.[15] Phase contrast tomography provides the real part of the relative refractive index, and image contrast is obtained in XGI from the first derivative of the phase shift. For the grating interferometry set-up, two gratings, namely beam-splitter grating G_1 and analyser grating G_2, are placed between the specimen and the detector, as illustrated in Figure 1 B. The first grating G_1 introduces periodic phase modulations into the wavefield, which is observed as an intensity periodic interference pattern in the detection plane of G_2.[3] G_2 consists of highly absorbing lines with the same periodicity as the interference pattern, and it detects distortions introduced by the sample.

2.3 X-Ray microtomography system

X-ray microtomography measurements were made using the nanotom® m (GE Sensing & Inspection Technologies GmbH) equipped with a 180 kV/15 W nanofocus® X-ray source with a spot size adjustable to between 0.9 µm and 2.7 µm. In order to evaluate interferometer performance, the measurements were performed with an acceleration voltage between 30 kV and 80 kV, beam currents between 50 µA and 650 µA and exposure times between 0.5 s and 9.0 s.

The source is operated in four modes with varying spot sizes.[8] For modes *"0", "1", "2", "3"* the source sizes are 2.0 - 2.7 µm, 2 µm, 1 µm and around 0.9 µm, respectively, as specified by the supplier.

Most laboratory XGI set-ups need three gratings, as the spot size is large. The advantage of a nanotom® m is the sufficiently small source size, thus ensuring coherence requirements are fulfilled,[16] in order to perform interferometric measurements in a two-grating configuration using a *Talbot* interferometer.

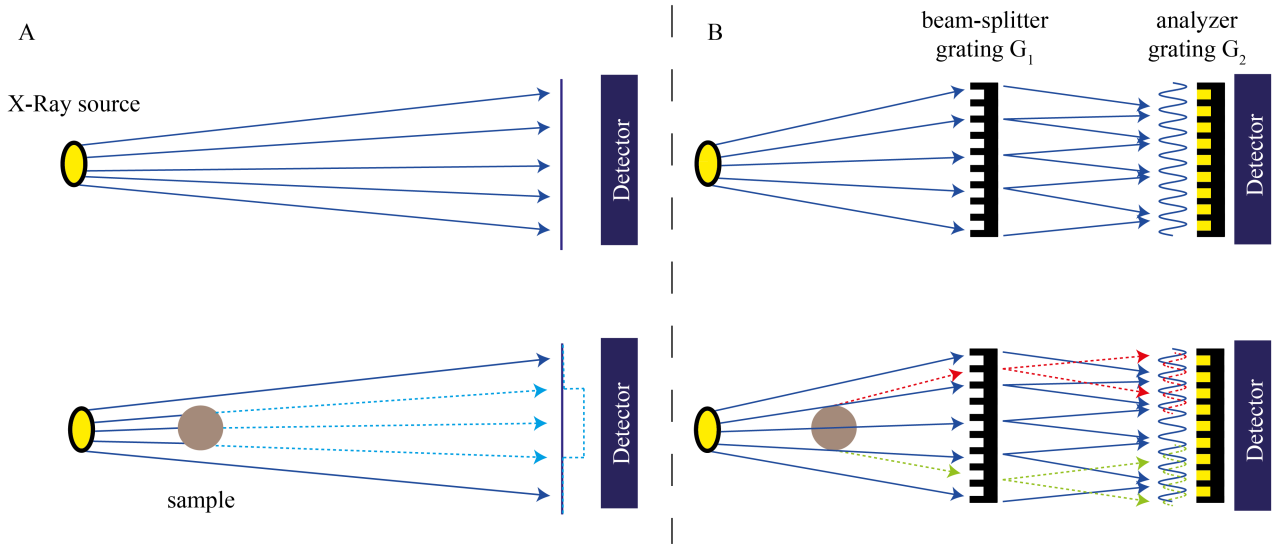

Figure 1. Schematics of µCT set-ups: absorption contrast (A) and grating-based phase contrast (B).

2.4 Grating interferometery

To extend the capability of the advanced laboratory µCT system achieving phase contrast, the µCT system was equipped with a grating-based, phase contrast set-up, as shown in Figure 2, consisting of a nano-positioning system (PI GmbH & Co, Karlsruhe, Germany), a three-axis positioning stage and a motorised goniometer (Optics Focus Instruments Co. Limited, Hong Kong, China).

The measurements were performed with two sets of round gratings, each 70 mm in diameter, in symmetric π-shift set-ups, see Table 1. Distances between the gratings of 29.6 cm and 21.7 cm correspond to the 1^{st} Talbot order. Both sets of gratings were fabricated for a design energy of 30 keV (Microworks GmbH, Karlsruhe, Germany).

Table 1. Grating parameters. G_{11}: beam-splitter grating of the first set-up; G_{21}: analyser grating of the first set-up; G_{12}: beam-splitter grating of the second set-up; G_{22}: analyser grating of the second set-up; duty cycle=a/b, see Figure 2, the ratio of grating structure width a to a grating period b.

Grating	G_{11}	G_{21}	G_{12}	G_{22}
Period [µm]	7.00	7.00	6.00	6.00
Duty cycle	0.51	0.42	0.55	0.50
Structure material	gold	gold	gold	gold
Structure height [µm]	6.00	85.00	5.74	60.07
Substrate	200 µm silicon	200 µm graphite	200 µm silicon	200 µm silicon

The interferometer operates in the phase-stepping mode. During the phase-stepping scan, G_2 is moved orthogonally to the X-ray propagation direction by the nano-positioning system. The positioning system is used for the precise alignment of G_1 and G_2. The interferometer is positioned in the µCT system between the detector and the sample holder, in front of the X-ray source.

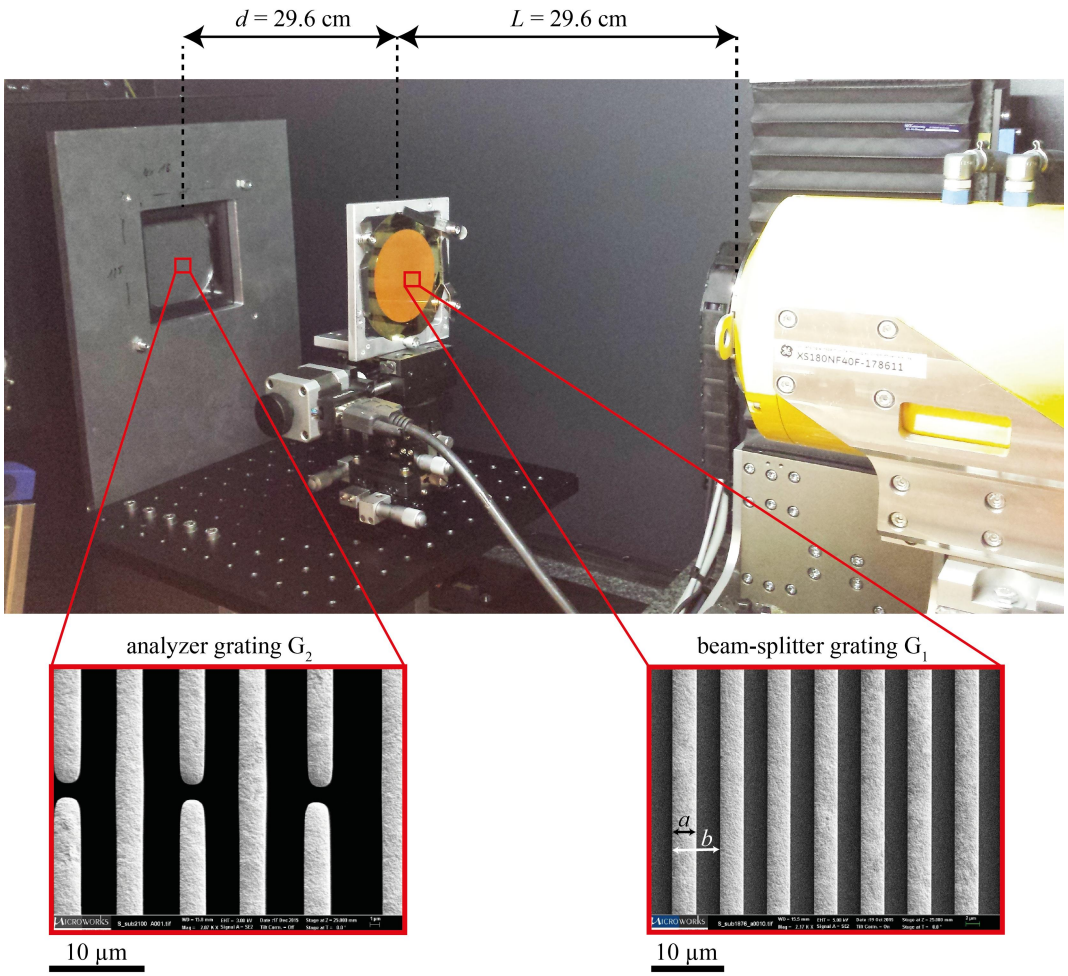

Figure 2. Extension of an absorption-based µCT system via a grating-based phase contrast set-up. The set-up consists of two gratings, G_1 and G_2. Scanning electron microscopy (SEM) images of both gratings, highlighting the finer details of their structure, are shown below. L: distance from the X-ray source to the beam-splitter grating G_1; d: distance from beam-splitter grating G_1 to analyser grating G_2; a: grating structure width; b: grating period.

3. RESULTS AND DISCUSSION

3.1 Visibility study

Efficiency of performance of interferometric set-up depends on many parameters. Visibility is an important parameter for the evaluation of the XGI set-up and is directly related to set-up efficiency. Based on the definition,[3] visibility V, see Figure 3 is

$$V = (I_{max} - I_{min})/(I_{max} + I_{min}) = A/O \tag{1}$$

where I_{max} and I_{min} are maximal and minimal values of intensity for the interference pattern, A is the amplitude of the stepping curve and O is the offset of the stepping curve.

Visibility depends on many parameters, including grating alignment and positioning as well as the X-ray spectrum, which in turn is dependent on acceleration voltage, filtering and source size.

Figure 4 (left) shows the results of visibility dependency over the selected beam currents and acceleration voltages plotted against mean photon counts in a 5×5 pixel window for the four source modes. The measurements were performed in seven phase steps over one period of interference pattern. For mode *"0"*, visibility was the

lowest and did not exceed 12 %. Visibility decreases when the spot size is decreased. In addition, intensity increases when the spot size increases. Mode *"1"* provides the best trade-off between intensity and visibility.

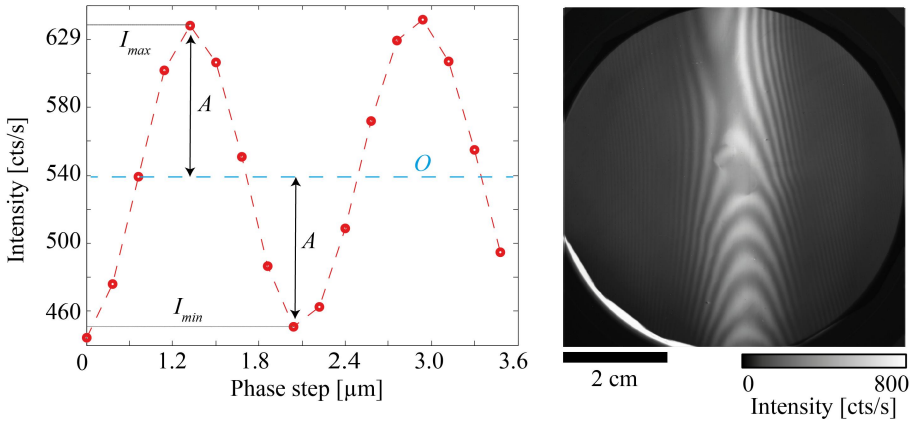

Figure 3. Definition of visibility. Intensity oscillations on a flat field and dark field corrected image during a phase stepping scan within a small 5×5 pixel window (left). Flat field and dark field corrected single phase step image (right). A: amplitude; O: offset. Both images are acquired with an acceleration voltage of 42 kV and a beam current of 315 µA.

Both sets of gratings were fabricated for a design photon energy of 30 keV. This design photon energy was selected as the best option for the simultaneous visualisation of soft and hard tissue samples[14] (see Holme et al. Table 1) with an average diameter of 5cm.[17–19] Acceleration voltages below 40 kV provide insufficient photon counts in the nanotom® m, and so an acceleration voltage of 42 kV, corresponding to photon energy of 30 keV based on theoretical calculations,[20] was selected as the design photon energy of the gratings.

The photon energy acceleration voltage relation is source type dependent. To verify for which acceleration voltage the highest visibility can be achieved, a visibility-voltage dependency experiment was performed for mode *"1"*, as shown in Figure 4 (right). For the 11 acceleration voltages within the ranges 30 kV to 70 kV, and the selected currents, projection data were recorded. Mean photon counts were kept constant for the experiments at around 500 before flat field and dark field correction. The imaging was performed with 17 phase steps over two periods of interference pattern. The highest visibility of 16.5 % was achieved for the 42 kV acceleration voltage. Strategies for visibility increase are now under consideration.

Visibility grows approximately linearly with the current, as illustrated in Figure 4 (left), while current decreasing at a constant voltage causes an increase in visibility, as we see in Table 2. Similar linear dependency can be obtained in terms of mean photon counts. This behaviour reflects the relation between source size and beam current.

Grating interferometry using synchrotron radiation is performed successfully with relatively short exposure times. X-ray tubes provide lower flux compared to synchrotron radiation sources, where exposure times of around 1 s for each phase step can be used,[21–23] which is why long exposure times are required[24] in order to produce quantitative phase images with a low-brilliance source. The visibility experiment, as shown in Figure 4 left, was performed with a total exposure time per phase step of 9 seconds. A decrease in time for one phase step is required in order to complete the tomography scan within a reasonable period of time.

In order to achieve high-resolution tomography with reasonable contrast, significant number of photons per detector pixel is required,[25] resulting in a radiation dose in the order of MGy per scan.[15] The reduction of a dose by decreasing exposure time or the number of phase steps would cause a noticeable drop in image quality. Such radiation exposure has biological effects on a sample; therefore, measurements should be performed post-mortem.

For mode *"0"* visibility is low, which is insufficient to generate useful projections. The minimum amount of counts necessary to see the specimen, based on the experiment, is 210 photons after flat field and dark field correction of the field of view. Based on the experimental results, the minimal visibility required to detect the specimen in alcohol solution was 15 %.

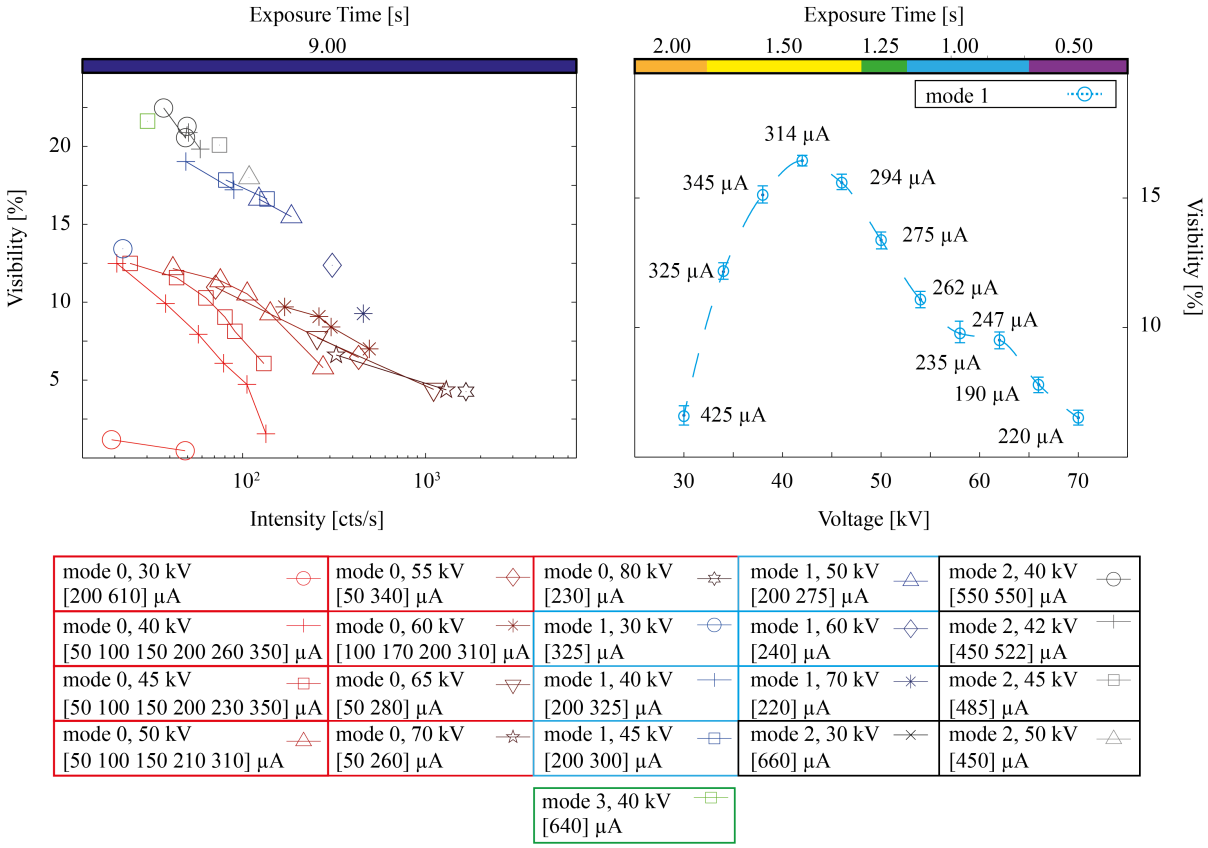

Figure 4. Dependency of visibility on the beam current and acceleration voltage for four source modes as a function of intensity (left). Visibility acceleration voltage dependency of mode *"1"* (right). Intensity: average photon counts over a 5×5 pixel window for which visibility was calculated after flat field and dark field corrections. In this context intensity is the same as the offset of the stepping curve, see Figure 3. With the colour bar on top, total exposure time is specified.

Table 2. Visibility dependency versus beam current for the selected voltages of mode *"0"* is given by linear relation: V=p1·I+p2. V: visibility [%]; U: source voltage; I_{min}: minimal current used for the experiment; I_{max}: maximal current used for the experiment; p1, p2: linear coefficients.

U [kV]	I_{min} [µA]	I_{max} [µA]	p1 [µA]	p2 [µA]
30	200	610	-0.003	3.02
40	50	350	-0.07 (-0.08 -0.06)	27.26 (24.89 29.62)
45	50	350	-0.04 (-0.05, -0.04)	27.16 (25.98, 28.34)
50	50	310	-0.05 (-0.07, -0.03)	27.61 (24.45, 30.77)
55	50	340	-0.03	23.48
60	100	310	-0.03 (-0.04, -0.02)	22.21 (20.18, 24.24)
65	50	280	-0.03	16.88
70	50	260	-0.02	14.28

Visibility is not the only parameter that determines how visible the sample is on projection data - sensitivity is also important. The highest specimen sensitivity was achieved for mode *"1"* between 40 kV and 50 kV acceleration voltage. For mode *"0"*, even intensities can be high, visibility low and the sample invisible. For mode *"2"* and *"3"*, despite the fact that visibility is high, the sample is invisible due to low counts. In addition,

there is noise which makes it problematic to visualise the sample. In order to detect a sample in projection data, sufficient visibility and intensity are needed. Based on the experimental results, the best-suited parameters were mode *"1"*, an acceleration voltage of 42 kV and a beam current of 315 µA. These parameters were used to acquire projection data.

3.2 Simultaneous visualisation of soft and hard tissues

Figure 5 presents projection data for a biological specimen consisting of hard and soft tissue parts, namely a chicken wing. The conventional absorption contrast image is shown in Figure 5 A and its magnified part D, and the differential phase contrast image is displayed in Figure 5 B and its magnified part C. We observe that phase contrast data yield better contrast for the soft part of the specimen, which in our case is marked with red arrows. Absorption contrast images show the contrast mainly dominated by bone, while the muscle layer structures are difficult to recognise.

In nature, structures that absorb X-rays highly, such as bone or other calcified parts, are often surrounded by weak X-ray absorbing tissue, such as muscles. X-ray micro-computed tomography of specimens containing both soft and hard tissues is challenging due to image artifacts, low absorption differences in soft tissues,[14] and optimal photon energy selection. XGI provide improved soft tissue contrast and helps determine 3D morphology down to true micrometer level. µCT systems extended towards phase contrast can enable the visualisation of a variety of samples within a laboratory environment, for example plaque-containing blood vessels for flow simulations.[14]

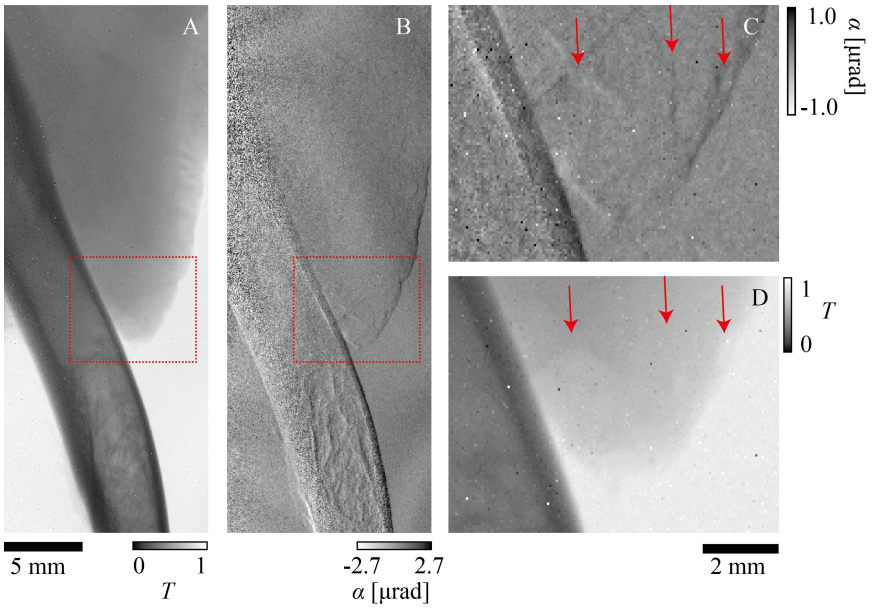

Figure 5. Simultaneous visualisation of soft and hard tissues. Absorption contrast *ABS* (A, D) and differential phase contrast *DPC* (B, C) projections of the lower part of a chicken wing. Red arrows indicate the points of superior *DPC* contrast over *ABS* contrast.

3.3 Hard tissue visualisation

Figure 6 presents projection data for a hard tissue specimen, namely the mandible of a pig. The phase contrast image is shown in Figure 6 A, the absorption contrast image in Figure 6 B, the dark-field image in Figure 6 C and the RGB colour-coded image in Figure 6 D. We observe that phase contrast data yield improved image quality in relation to bony tissue surrounding the implant; however, information from the implant itself is not provided. The dark-field and absorption contrast projections enhance contrast for the bony part of the sample.[3] Energy for the accurate visualisation of the Ti implant is insufficient.[26]

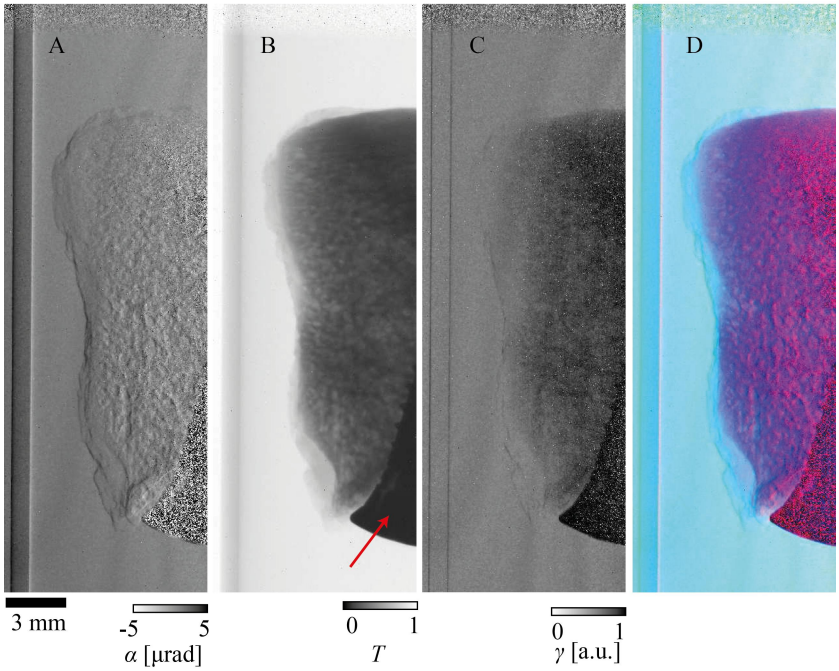

Figure 6. Visualisation of a hard tissue specimen: the mandible cylindrical block of a pig with a Ti-implant, marked by the red arrow. A: phase contrast image *DPC*; B: absorption contrast image *ABS*; C: dark-field image *DCI*; D: combined RGB colour-coded image, where *DPC* data is coded in the red channel, *ABS* in the green and *DCI* in the blue. α: deflection angle; T: transmission; γ: scattering.

Visualisation of hard tissue components with implants is a complex, as it usually yields severe streak artifacts.[27] Figure 6 D demonstrates that the combination of DPS, ABS and *DCI* images with straightforward registration allows for significant information gain.

3.4 3D visualisation of spiders

Figures 7 and 8 present projections of biological specimens, in particular the selected alcohol-fixed spiders *Hogna radiata* (*Fam. Lycosidae*) and *Xysticus erraticus* (*Fam. Thomisidae*). An external visual inspection does not provide information about the internal structure, as seen in Figures 7 A and 8 A. Conventional absorption contrast images are shown in the images of Figures 7 C and 8 B, D, and the differential phase contrast is apparent in Figures 7 B and 8 C. We observe that phase contrast data yield better contrast for the specimen, and provide a higher amount of information than absorption contrast data equal in pixel size.

The locomotion system of biological creatures is a significant source of innovation and inspiration. In contrast to humans, insects can climb various surfaces or survive in severe environmental conditions, and so mimicking these principles is of particular interest in areas such as robotics.[11,12] The micro-hydraulic system used by spiders to extend their legs has the potential to be used in space applications.[28] Replicating creatures such as spiders is a complicated task, and therefore advanced research using modern observation equipment is required.[11] Phase contrast hard X-ray imaging is a modality that can bring significant benefits, thereby allowing the visualisation of softer and harder components simultaneously and producing information with isotropic micrometer resolution.

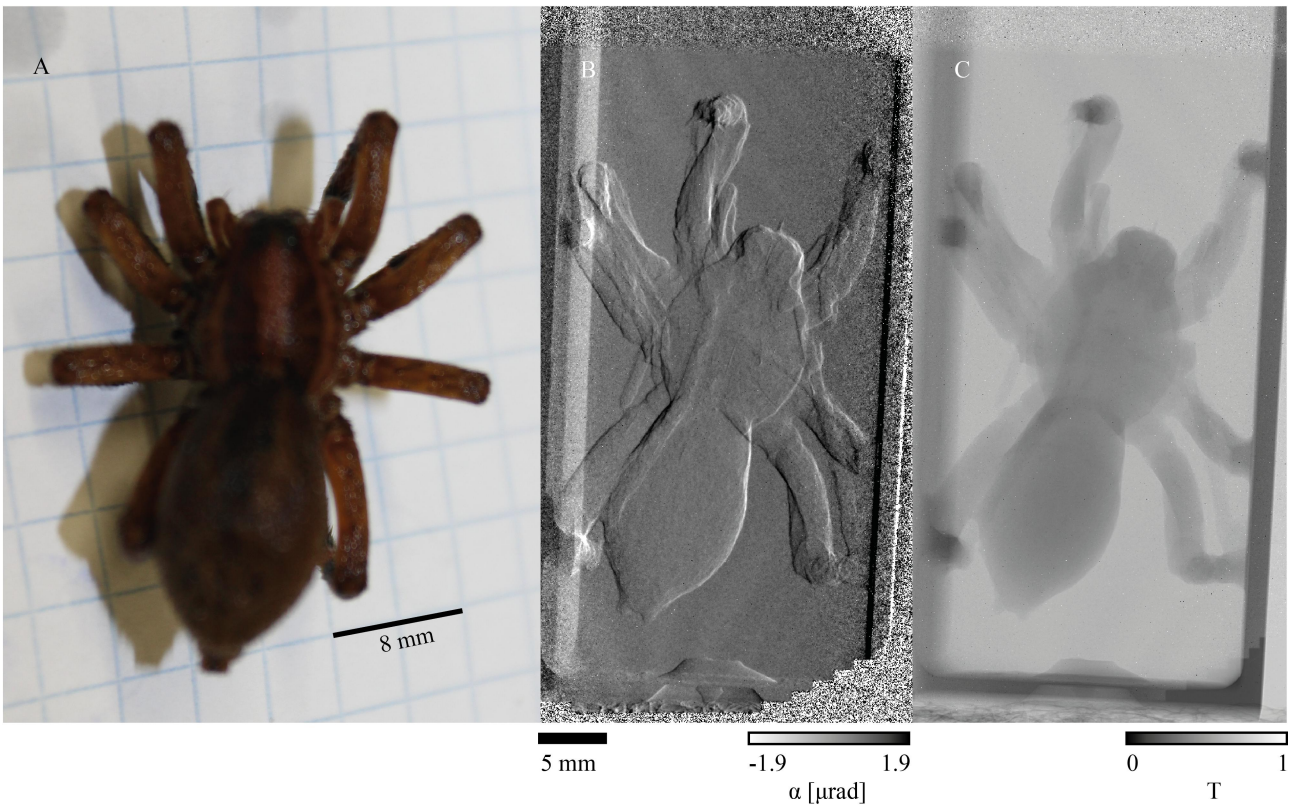

Figure 7. Visualisation of *Hogna radiata* (*Fam. Lycosidae*): photograph (A), differential phase contrast *DPC* (B) and absorption contrast *ABS* (C) images. The *DPC* and *ABS* images are extracted from the same phase-stepping scan. α: deflection angle; T: transmission, where 0 is 0 % transmission and 1 is 100 % transmission.

4. SUMMARY AND OUTLOOK

Hard X-ray grating interferometry provides complementary information to conventional absorption contrast data, namely phase shift and scattering, and plays a particularly important role in soft tissue visualisation or the simultaneous visualisation of soft and hard tissues. Based on an improved understanding of the architecture of the human body down to the micrometer scale, future medical implants will incorporate far more biomimetic principles and thus be of greater benefit to patients.

Grating-based phase contrast is a quantitative 3D imaging method. Consequently, it provides a sound basis for bioinspiration and biomimetics, allowing for the quantitative comparison of biofabricated products with their natural counterparts.

In this work we have evaluated the performance of a grating interferometer in a laboratory-based µCT system. The projection data established herein already provide significantly more complementary information compared to conventional absorption contrast. The question arises to what extent laboratory-based phase contrast tomography can provide results comparable to synchrotron radiation-based phase contrast tomography.

The current work presents the results of evaluating XGI on projection data. In the next step, sample projections will be reconstructed by employing a tomography algorithm, and image reconstruction will enable a comprehensive 3D analysis of a variety of samples.

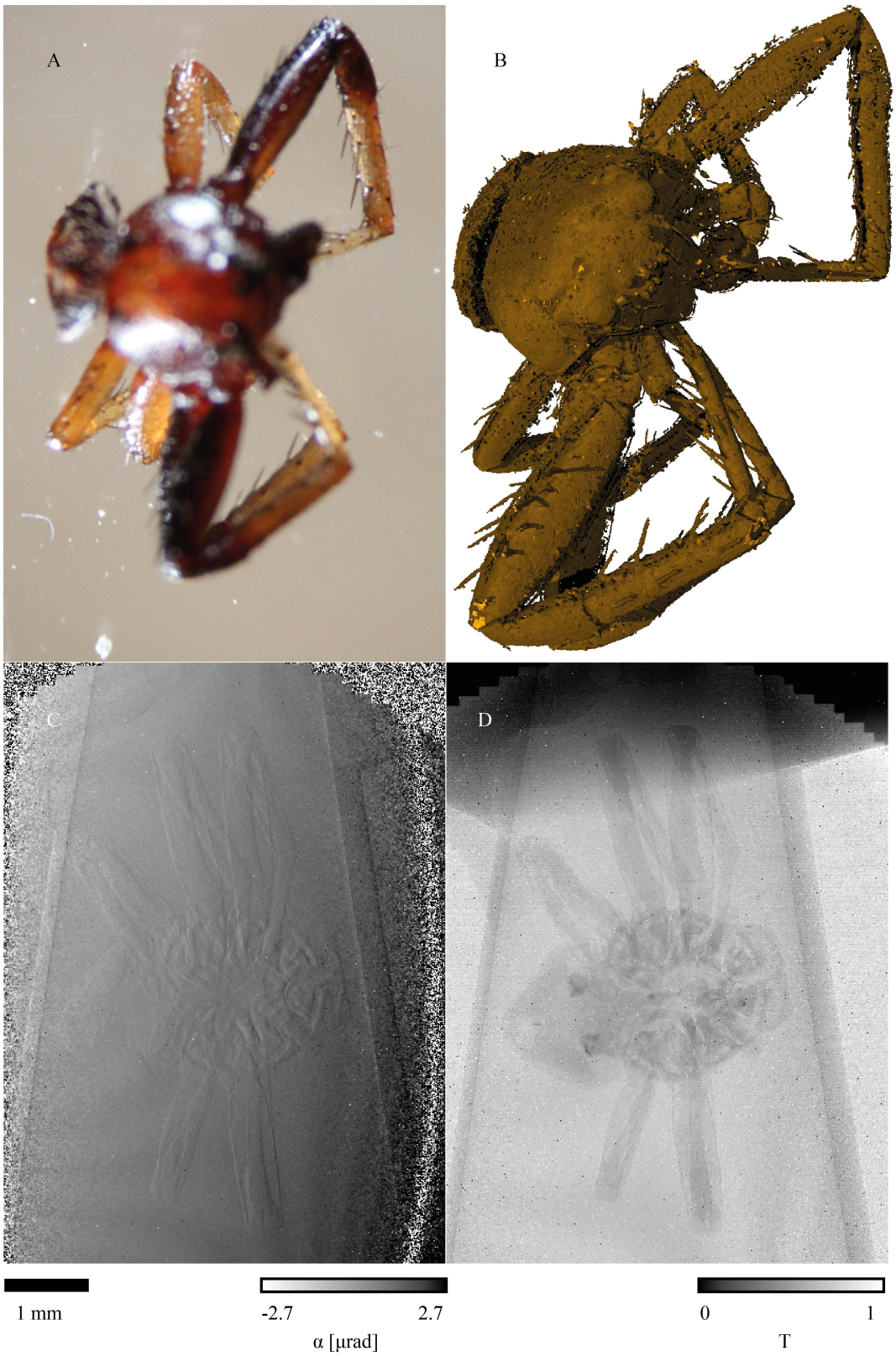

Figure 8. Visualisation of *Xysticus erraticus* (*Fam. Thomisidae*): microphotograph (A), 3D absorption contrast volume rendering (B), differential phase contrast (C) and absorption contrast images (D). α: deflection angle; T: transmission.

5. ACKNOWLEDGEMENTS

The authors gratefully acknowledge the financial support of the Swiss National Science Foundation (SNSF) projects 147172 and SNSF R'Equip project 133802. Grating fabrication was carried out with the support of the Karlsruhe Nano Micro Facility (KNMF, www.kit.edu/knmf). The support of Ambros Hänggi from Naturhistorisches Museum Basel, Switzerland, is also highly appreciated.

REFERENCES

[1] Gruber, P., Gebeshuber, I., Stachelberger, H., Hellmich, C., Bruckner, D., and Schmiedmayer, H.-B., [*Biomimetics - Materials, Structures and Processes: Examples, Ideas and Case Studies (Biological and Medical Physics, Biomedical Engineering)*], 1–9, Springer, New York (2011).

[2] Bar-Cohen, Y., [*Biomimetics: Nature-Based Innovation*], 431–445, CRC Press Inc., Boca Raton, 1st ed. (2011).

[3] Pfeiffer, F., Herzen, J., Willner, M., Chabior, M., Auweter, S., Reiser, M., and Bamberg, F., "Grating-based X-ray phase contrast for biomedical imaging applications," *Z. Med. Phys.* **23**(3), 176–185 (2013).

[4] Deyhle, H., Weitkamp, T., Lang, S., Schulz, G., Rack, A., Zanette, I., and Müller, B., "Comparison of propagation-based phase-contrast tomography approaches for the evaluation of dentin microstructure," *Proc. SPIE* **8506**, 85060N (2012).

[5] Dziadowiec, I., Beckmann, F., Schulz, G., Deyhle, H., and Müller, B., "Characterization of a human tooth with carious lesions using conventional and synchrotron radiation-based micro computed tomography," *Proc. SPIE* **9212**, 92120W (2014).

[6] Müller, B., Germann, M., Jeanmonod, D., and Morel, A., "Three-dimensional assessment of brain tissue morphology," *Proc. SPIE* **6318**, 631803 (2006).

[7] Wenz, J., Schleede, S., Khrennikov, K., Bech, M., Thibault, P., Heigoldt, M., Pfeiffer, F., and Karsch, S., "Quantitative X-ray phase-contrast microtomography from a compact laser-driven betatron source," *Nat. Commun.* **6**, 7568 (2015).

[8] Brunke, O., Brockdorf, K., Drews, S., Müller, B., Donath, T., Herzen, J., and Beckmann, F., "Comparison between X-ray tube-based and synchrotron radiation-based μCT," *Proc. SPIE* **7078**, 70780U (2008).

[9] Pfeiffer, F., Weitkamp, T., Bunk, O., and David, C., "Phase retrieval and differential phase-contrast imaging with low-brilliance X-ray sources," *Nat. Phys.* **2**(4), 258–261 (2006).

[10] Bech, M., Jensen, T., Bunk, O., Donath, T., David, C., Weitkamp, T., Le Duc, G., Bravin, A., Cloetens, P., and Pfeiffer, F., "Advanced contrast modalities for X-ray radiology: Phase-contrast and dark-field imaging using a grating interferometer," *Z. Med. Phys.* **20**(1), 7–16 (2010).

[11] Gasparetto, A., Vidoni, R., and Seidl, T., "Kinematic study of the spider system in a biomimetic perspective," *Proc. IEEE/RSJ IROS* , 3077–3082 (2008).

[12] http://www.megahard.pro/design-portfolio/spider robot, "Megahard: Spider robot."

[13] Luckow, M., Deyhle, H., Beckmann, F., Dagassan-Berndt, D., and Müller, B., "Tilting the jaw to improve the image quality or to reduce the dose in cone-beam computed tomography," *Eur. J. Radiol* **80**(3), e389–e393 (2011).

[14] Holme, M., Schulz, G., Deyhle, H., Weitkamp, T., Beckmann, F., Lobrinus, J., Rikhtegar, F., Kurtcuoglu, V., Zanette, I., Saxer, T., and Müller, B., "Complementary X-ray tomography techniques for histology-validated 3D imaging of soft and hard tissues using plaque-containing blood vessels as examples," *Nat. Protoc.* **9**(6), 1401–1415 (2014).

[15] Lang, S., Zanette, I., Dominietto, M., Langer, M., Rack, A., Schulz, G., Le Duc, G., David, C., Mohr, J., Pfeiffer, F., Müller, B., and Weitkamp, T., "Experimental comparison of grating- and propagation-based hard X-ray phase tomography of soft tissue," *J. Appl. Phys.* **116**, 15 (2014).

[16] Weitkamp, T., David, C., Kottler, C., Bunk, O., and Pfeiffer, F., "Tomography with grating interferometers at low-brilliance sources," *Proc. SPIE* **6318**, 63180S (2006).

[17] Schulz, G., Weitkamp, T., Zanette, I., Pfeiffer, F., Beckmann, F., David, C., Rutishauser, S., Reznikova, E., and Müller, B., "High-resolution tomographic imaging of a human cerebellum: comparison of absorption and grating-based phase contrast," *J. R. Soc. Interface* **7**(53), 1665–1676 (2010).

[18] Grodzins, L., "Critical absorption tomography of small samples. Proposed applications of synchrotron radiation to computerized tomography II," *Nucl. Instr. Meth. Phys. Res.* **206**(3), 547–552 (1983).

[19] Grodzins, L., "Optimum energies for x-ray transmission tomography of small samples. Applications of synchrotron radiation to computerized tomography I," *Nucl. Instr. Meth. Phys. Res.* **206**(3), 541–545 (1983).

[20] Malecki, A., "JGratingCalc: http://www.e17.ph.tum.de/index.php/services/software/110.html."

[21] Buscema, M., Holme, M., Deyhle, H., Schulz, G., Schmitz, R., Thalmann, P., Hieber, S., Chicherova, N., Beckmann, F., Herzen, J., Weitkamp, T., Saxer, T., and Müller, B., "Grating interferometry-based phase microtomography of atherosclerotic human arteries," *Proc. SPIE* **9212**, 921203 (2014).

[22] Hieber, S., Khimchenko, A., Kelly, C., Mariani, L., Thalmann, P., Schulz, G., Schmitz, R., Greving, I., Dominietto, M., and Müller, B., "Three-dimensional imaging of human hippocampal tissue using synchrotron radiation- and grating-based micro computed tomography," *Proc. SPIE* **9212**, 92120S (2014).

[23] Schulz, G., Dominietto, M., Kovacs, Z., Schmitz, R., Hieber, S., Thalmann, P., Beckmann, F., and Müller, B., "Tumors in murine brains studied by grating-based phase contrast microtomography," *Proc. SPIE* **9212**, 92120Q (2014).

[24] Wu, Z., Wang, Z., Gao, K., Ge, X., Wu, Z., Chen, H., Wang, S., Zhu, P., Yuan, Q., Huang, W., and Zhang, K., "X-ray phase radiography and tomography with grating interferometry and the reverse projection technique," *J. Phys. D* **46**(49), 494003 (2013).

[25] Starodub, D., Rez, P., Hembree, G., Howells, M., Shapiro, D., Chapman, H., Fromme, P., Schmidt, K., Weierstall, U., Doak, R., and Spence, J., "Dose, exposure time and resolution in serial X-ray crystallography," *J. Synchrotron. Radiat.* **15**(1), 62–73 (2007).

[26] Cattaneo, P., Dalstra, M., Beckmann, F., Donath, T., and Melsen, B., "Comparison of conventional and synchrotron radiation based microtomography of bone around dental implants," *Proc. SPIE* **5535**, 757–764 (2004).

[27] Berndt, D., Luckow, M., Lambrecht, J., Beckmann, F., and Müller, B., "Quality assessment of clinical computed tomography," *Proc. SPIE* **7078**, 70780N (2008).

[28] Menon, C. and Lira, C., "Active articulation for future space applications inspired by the hydraulic system of spiders," *Bioinspir. Biomim.* **1**(2), 52–61 (2006).